Thermodynamic and economic investigation of a screw expander-based direct steam generation solar cascade Rankine cycle system using water as thermal storage fluid

Jing Li[1, 3], Pengcheng Li[2], Guangtao Gao[1], Gang Pei[1]*, Yuehong Su[3], Jie Ji[1]

[1]*Department of Thermal Science and Energy Engineering, University of Science and Technology of China, 96 Jinzhai Road ,Hefei, China*

[2]*School of Automobile and Traffic Engineering, Hefei University of Technology,193 Tunxi Road, Hefei, China*

[3]*Department of Architecture and Built Environment, University of Nottingham, University Park, Nottingham, NG7 2RD, UK*

Abstract: Solar electricity generation system (SEGS) which employs cascade steam-organic Rankine cycle (SORC) and steam screw expander (SE) is promising due to the high efficiency at moderate heat source temperature. This paper puts a special emphasis on heat storage and thermo-economic evaluation. Preferable operating temperature of the system is first clarified on the basis of SE characteristics. The temperature-dependent permissible stress of steam accumulator is modelled and the capital cost is investigated. Comparison between the direct steam generation (DSG) SEGS and an indirect one using thermal oil is made at a power capacity of 1 MW and storage of 6.5 hours. The results indicate the DSG system has both thermodynamic and economic superiorities. The hot side temperature (T_H) of SORC generally does not exceed 250 ℃ to achieve an optimum solar thermal power efficiency. Given radiation of 750 W/m², the maximum

efficiency ($\eta_{T,m}$) is 14.3% with a corresponding T_H around 240 ℃. The material cost of pressure vessels is 2.55 million RMB. For the indirect system, the optimal T_H is about 230 ℃ and $\eta_{T,m}$ approximates to 13.2% and the estimated oil cost is 7.92 million RMB. It is recommended to adopt steam accumulators in the SE-driven SEGS.

Keywords: solar thermal power generation; screw expander; thermal storage; steam accumulator; part-load behavior

*Corresponding author. Tel. /Fax: +86 551 63607367. E-mail: peigang@ustc.edu.cn.

1．Introduction

Screw expander (SE) is a volumetric machine used for the production of mechanical work in the power interval from several kW to a few MW. The functional characteristics of SE differ significantly from those of dynamic expanders (e.g. turbines). SE has high tolerance for two-phase working fluid and the fluctuation of heat source in a wide range of pressure, temperature and volumetric flow. It is able to start up and shut down quickly, and has no special warm-up, less faults from over-speeding and turning.

SE technology is promising in the low-medium temperature applications. The SE industry is at a stage for promotion in the world, with major industrial suppliers including Jiangxi Huadian Electric Power Co.,Ltd, Opcon Group, Kaishan Ltd., Denair Group, ElectraTherm, Shanghai Hanbell Precise Machinery, Heliex Power Ltd. and QiyaoExpander Ltd. Products such as Opcon Powerbox WST (100-1600 kW) [1], HP145/HP204 (160-500 kW) [2], SEPG (300-3000 kW) [3], LGP510-S (750-2500

kW) [4], KE110V-50 (60-1000 kW), 6500-FL(110 kW) [5] and Denair ORC (10-300 kW or above) [6] are available on the markets. Isentropic efficiency of 75-80% is claimed for most products. The SE-based plants are gaining ever increasing interest as cost-effective sustainable energy systems.

Solar electricity generation system (SEGS) holds a potential market for SE [7-10]. SEGS using steam SE avoids superheat at the expander inlet [11]. Direct steam generation (DSG) in the parabolic trough collectors (PTCs) can be facilitated. The system can work at lower temperature than steam turbine-driven ones without remarkable decrement in the efficiency. The technical requirement in solar energy collection is thus reduced. Coupling with a bottom organic Rankine cycle (ORC), the SE does not need to experience highly off-design operation [12-14], and the SEGS can perform better at low ambient temperature. It is especially suitable for distributed cogeneration applications. Fundamentals, advantages and some thermodynamic results of the SEGS using cascade steam-organic Rankine cycle (SORC) at constant SE efficiency have been presented previously [15].

Heat storage is a key subject in solar thermal electricity generating systems. The proposed SEGS is appreciated only if the issues related with storage can be easily addressed. Similarly with steam turbine-driven systems, there are many alternative materials for thermal storage of the SE-based SEGS, including molten salt, thermal oil and water.

Molten salts were adopted for thermal energy storage in Themis solar power plant in 1983. Salts composed of $NaNO_3$ (w_t=60%) and KNO_3 (w_t=40%) were chosen as

storage mediums of Solar Two in 1995 [16]. Molten salts acting as the heat transfer and storage fluid were further employed in Solar Tres power plant built in 2008 [17]. After a long-term development, molten salt technology represents one of the most flexible, efficient and cost-effective large-scale solar energy storage technologies nowadays and is being deployed in many plants such as 280 MW Solana Generating Station and Ivanpah concentrating solar power plant.

Thermal oil was used for storage in the first SEGS plant (SEGS I) in 1984. It was filled into two different tanks: a hot tank, where the oil was stored after being heated to 307 °C by the collectors, and a cold tank, where the oil was kept at about 240°C after releasing its energy to the Rankine cycle [18-19]. This storage technology was found to be successful for helping the plant dispatch its electricity generation during non-sunlight periods. Another benefit was that oil could be utilized as heat transfer fluid. Because thermal stability of commercial thermal oil could be guaranteed only when the working temperature ranged below 395 °C, this storage concept no longer appeared in later, more efficient SEGS plants.

Water was especially suitable to meet the requirements for buffer storage in solar steam systems. Pros and cons of steam accumulator for thermal storage of conventional turbine-driven SEGSs have been estimated [20-24]. Water was selected as the storage, heat transfer and working fluid in commercial solar power plants of Abengoa Solar's Planta Solar 10 and 20 (PS10 and PS20). In PS10, the design temperature and pressure of the steam accumulators were 250 °C and 4 MPa, respectively. The storage system consisted of four tanks that were sequentially

operated in relation to their charge status [25]. In PS20, the design values were elevated to 300 °C and 4.5 MPa [26]. The introduction of steam accumulators eliminated intermediate heat transfer fluid and steam generator. The storage system could react fast to transience in radiation without complicated control strategy.

Experience in SEGSs indicates that molten salt is the best choice for thermal storage in the high temperature application (> 400 °C) [27]. Thermal oil is attractive in the temperature range from 300 °C to 400 °C. And both thermal oil and water are appropriate medium at temperature below 300 °C. Notably, so far thermal storage for SEGS is affected by the characteristics of steam turbine. Due to the technical difficulty and short lifetime of turbine operating with wet steam, a large degree of superheat (>100 °C) at the device inlet is favorable. This will reduce the solar power efficiency at a given heat source temperature. For the sake of efficiency improvement and cost-effectiveness, SEGS tends to move towards higher operating temperature (>500 °C). As the most promising medium in such application, molten salt is currently receiving great interest [28-33].

In case of SE, the problems associated with wet steam are overcome. It is unnecessary to harness solar energy at temperature above 400 °C to implement efficient power conversion. A solar electricity efficiency around 15% can be expected with heat source of just 250 °C [15]. In this situation, steam accumulator rather than molten salt will be a competitive method.

It is innovative to couple the steam screw expander-based SORC with DSG solar collectors and water heat storage. Thermo-economic performance of this sort of

system has not been reported and it is worth examining its feasibility. Meanwhile detailed investigation of the thermo-mechanical stress in storage vessel and the mathematical relationship between operating temperature/pressure and consumption of material (i.e. steel) are rare. Quantitative analysis of the capital cost of pressure vessel working with steam for solar energy storage in the temperature range from 200 °C to 250 °C is needed and valuable.

This paper focuses on the steam SE-based solar thermal electricity system with water as the heat transfer and storage fluid. It aims to explore the applicability of this storage technology in the proposed SEGS. The main contributions are as follows.

(1) Advantages of the system are outlined.

(2) Mathematical model on the steam accumulator is established. Influence of key factors on the accumulator cost is analyzed. Valuable information on the cost of pressure vessel operating within the recommended temperature limit is presented.

(3) Thermodynamic and economical comparisons between the SEGSs using water and thermal oil as the storage fluids, are conducted. The superiority of the former is clarified.

(4) Annual performance, part-load behavior and storage cost of the SE-assisted SEGS are evaluated, giving a better understanding of the system.

2. Characteristics of screw expander

The optimum working condition of the system is rooted on the current technology of SEs, which possess some characteristics that have significant effect on the operation

of SEGS, including:

(1) Allowance for flexible multi-phase expansion. SE is a kind of full-flow power machine, which can accept not only superheated and saturated steam (or vapor in case of organic fluid), but also wet steam and steam-liquid mixtures. Unlike the mode of power conversion in turbines, the velocity of fluid in SEs is much lower and merely a relatively small portion of power is facilitated by dynamic effects relevant to fluid motion. Hence the presence of liquid droplets in the machine has little influence on its lifetime.

(2) Low built-in expansion ratio. A small built-in expansion ratio is desirable because it maximizes the input flow of fluid, before the high pressure port is cut off. Great mass flow rate can diminish the effect of leakage [34]. Nevertheless, it leads to under expansion and expulsion of the fluid at a too high pressure. Available work is thus lost and the expander efficiency falls. There is a compromise between the manufacturing cost and the work loss. According to the existing plants, common built-in expansion ratio of SE is around 4.

(3) Excellent part-load behavior. Low built-in expansion ratio is not a good match for the practical one, which usually exceeds 10 in light of the heat source and heat sink temperatures. Fortunately, this can be compensated by the excellent part-load behavior of SE. Many works have demonstrated this feature [35-37]. The SE can operate efficiently to a large extent of pressure ratio (r_p). The decline of isentropic efficiency from the maximum is only about 10% when the operating r_p increases by three times as the built-in [38].

(4) Limited pressure difference. SE is positive displacement rotary machine comprising a meshing pair of helicoid lobed rotors on parallel axes, contained in a casing. Pressure difference across the rotors may impose heavy loads on them and cause rotor deformation. As a result, the pressure difference at which SE can function reliably and economically is restricted. Most commercial SEs have a maximum operating pressure below 4.0 MPa. This constraint is similar to screw compressors which have been widely used in low-medium pressure applications.

3**. System description**

Fig.1 shows the DSG solar power system using SE. Steam is generated in the PTCs. The power conversion subsystem is the cascade SORC. Cycle I (red color) and Cycle II (blue color) are the steam Rankine cycle (SRC) and ORC, respectively. Cycle I mainly consists of SE, condenser (HX1), pumps (P1, P3), steam accumulator (water storage unit) and collectors. Cycle II is composed of expander, condenser (HX2), pump (P2). Regarding the properties of common organic fluids, turbine is a better option in the ORC [15].

HX2 is the heat exchanger between the ORC fluid and the environment. Water cooling is preferable than air cooling on account of larger temperature difference driving the ORC and smaller negative power consumption. To support space heating and absorption cooling, heat exchangers can be placed in parallel with HX1. HX1 serves as the evaporator for Cycle II. Both SRC and ORC fluids undergo phase change in HX1. The outlet temperature, pressure and quality of the fluids are affected by the heat transfer inside. Three aspects could be considered for the feasibility of

HX1. First, commissioning is one practical action before the system works on the nominal condition. In this process, auxiliary devices such as sensor, controller, by-pass, liquid-vapor separator and reservoir are needed [39], which may shorten commissioning time. Second, cascade Rankine cycle using mercury and steam had been employed in historical power systems and similar heat exchangers as HX1 were included [40], though the plants were limited probably because of high capital cost and the obvious toxic hazard if the mercury leaked into the environment. Third, nowadays cascade refrigeration cycle is used in low temperature applications where a common single-refrigerant two-stage compression system gets inefficient [41]. The internal heat exchanger plays a key role in the system and its outlet fluid in the high-temperature circuit should not contain liquid for the proper operation of the compressor. The experience in cascade refrigeration cycle reinforces the applicability of HX1 in the SORC.

The operation is flexible and the system has many operating modes including:

a. Simultaneous heat collection and power conversion (Mode 1). V1, V2 and V3 are open, and P1 and P2 work. Water is heated and vaporized in PTCs. Saturation steam goes into the SE, exporting power during expansion. The exhaust is condensed to saturation liquid in HX1, and is pressurized and sent back by P1 to the PTCs. The condensation heat is used to vaporize the working fluid in the ORC.

b. Heat storage in process (Mode 2). V3 and V4 are open and P3 runs. Solar energy is stored in the form of water sensible heat.

c. Sole power conversion (Mode 3). When solar radiation is unavailable and power is demanded, V1, V2, V5 are open. P1 and P2 run. Heat is released by water and converted into power.

d. Simultaneous heat collection, power conversion and heat storage (or release) (Mode 4). This mode is more complicated but also more common in practice. V1, V2, V3 and V4 are open. P1, P2 and P3 run. The design area of PTCs is relevant to the nominal power and capacity factor of the plant. In case of strong solar radiation, heat collected by PTCs is partly used to generate power and the rest is stored in the accumulator. While under weak radiation the input energy may be not sufficient for power conversion and heat is released from the accumulator. In both situations the SORC operates smoothly. Depending on solar radiation, the mass flow rate through P3 is adjustable. Water leaving the solar field can be at liquid, binary or vapor state. Superheat is prevented in a simple way.

In contrast to the conventional turbine-driven DSG solar thermal power system, superheater is eliminated. Moreover, the technical problems associated with steam accumulator can be more easily solved. For conventional systems the investment cost on water storage is dominated owing to the vessel operating at high temperature and pressure which may reach 400 °C and 10 MPa [24]. Since water is used as both storage medium and working fluid, high discharge rate is possible and the capacity is limited by the vessel volume. There is a decline in pressure during the discharge process, which would lead to degradation of the turbine performance. These concerns are eased in the present of SE because it operates at relatively lower temperature and

pressure, and has excellent part-load performance.

The representative two-tank heat transfer fluid (HTF) system is shown in Fig. 2. Thermal oil is used as the HTF and heat storage medium, which is a proven technology applied in some SEGS plants for two decades without major troubles. Thermal oil seems to be the best HTF in regard to the operational aspect, safety and cost [42].

A typical thermodynamic process of the cascade cycle is illustrated in Fig.3. The numbers are linked with those in Figs.1 and 2.

4. Mathematical models

4.1. Solar energy collection efficiency

It will be shown in the following sections that collectors in both DSG and HTF systems operate at pressure less than 4 MPa, and most commercial PTCs should be applicable. Therefore, it is assumed in this work that the systems in comparison employ the same kind of collectors. A type of PTC installed in the USA with up to 2700 m^2 of aperture area is referenced here [43]. The performance formula of a single PTC provided by the manufacturer is [44]:

$$\eta_{PTC}(T) = 0.762 - 0.2125 \times \frac{T - T_a}{G_b} - 0.001672 \times \frac{\left(T - T_a\right)^2}{G_b} \tag{1}$$

where G_b is beam solar radiation ; T is collector inlet temperature.

Thousands of collectors are usually adopted in SEGS, the temperature difference between neighboring collectors is supposed to be small. To calculate the overall efficiency for solar energy collection, it is reasonable to assume that the average operating temperature of the collector changes continuously from one module to

another.

For thermal oil and water at liquid state, in order to reach an outlet temperature T_{out} with an inlet temperature T_{in}, the required collector area is obtained by

$$A_l = \int_{T_{in}}^{T_{out}} \frac{m_1 \cdot C_p(T)}{\eta_{PTC}(T) \cdot G_b} dT \tag{2}$$

where m_1 is mass flow rate of oil or water through the collectors. For the DSG system, it is also the mass flow rate in SRC.

Heat capacity of oil or water can be expressed by a first order approximation:

$$C_p(T) = C_{p,0} + \alpha(T - T_0) \tag{3}$$

Where $C_{p,0}$ is heat capacity corresponding to a reference temperature T_0.

With $c_1 = 0.2125 / G_b$, $c_2 = 0.001672 / G_b$, the collector area according to Eqs. (1) - (3) is calculated by

$$A_l = \frac{m_1}{c_2 G_b (\theta_2 - \theta_1)} \left[(C_{p,a} + \alpha\theta_1) \ln \frac{(T_{out} - T_a - \theta_1)}{T_{in} - T_a - \theta_1} + (C_{p,a} + \alpha\theta_2) \ln \frac{\theta_2 - T_{in} + T_a}{\theta_2 - T_{out} + T_a} \right] \tag{4}$$

Eq.(4) is the analytic solution to the formula of integration of Eq.(2). c_1 and c_2 are two defined intermediate parameters. θ_1 and θ_2 are the arithmetical solutions of Eq. (5) （$\theta_1 < 0$, $\theta_2 > 0$）.

$$0.762 - c_1\theta - c_2\theta^2 = 0 \tag{5}$$

$$C_{p,a} = C_{p,0} + \alpha(T_a - T_0) \tag{6}$$

θ_1 and θ_2 can be determined once solar radiation is known since Eq.(5) is a common quadratic function.

Collector efficiency in liquid phase region is calculated by

$$\eta_{PTC,l} = \frac{m_1 \Delta h_l}{G_b A_l} \tag{7}$$

Eq. (7) is adequate to calculate the solar energy collection efficiency of HTF system. For DSG system, the solar field contains steam-liquid mixture. Overall collector efficiency is calculated by Eq. (8)

$$\eta_{PTC} = \frac{Q}{G_b(A_l + A_b)} = \frac{\Delta h_l + \Delta h_b}{\dfrac{\Delta h_l}{\eta_{PTC,l}} + \dfrac{\Delta h_b}{\eta_{PTC,b}}} \tag{8}$$

where Δh_l and Δh_b are the enthalpy increments of water in liquid phase and binary phase regions. $\eta_{PTC,b}$ can be easily calculated since the temperature is constant.

4.2. Power conversion efficiency

4.2.1. Expanders

The work generated by SE or turbine is defined as Eq. (9) or Eq. (10):

$$W_{SE} = m_I(h_1 - h_2) = m_I(h_1 - h_{2s})\varepsilon_{SE} \tag{9}$$

$$W_T = m_{II}(h_5 - h_6) = m_{II}(h_5 - h_{6s})\varepsilon_T \tag{10}$$

4.2.2. Heat exchanger

Heat balance in HX1 is expressed by

$$m_I(h_2 - h_3) = m_{II}(h_5 - h_8) \tag{11}$$

4.2.3. Pumps

The work required by pump is expressed by

$$W_{p1} = m_I(h_4 - h_3) = m_I(h_{4s} - h_3)/\varepsilon_p \tag{12}$$

$$W_{p2} = m_{II}(h_8 - h_7) = m_{II}(h_{8s} - h_7)/\varepsilon_p \tag{13}$$

The pressure drop through the collectors, heat exchangers and pipes are neglected. Flow resistance in the PTCs is supposed to have limited effect on the net power

output of the system. For example, if the design pressure at the SE inlet is 4.0 MPa

and the pressure loss in the PTCs is 0.5 MPa, then the outlet pressure of P1 will just

need to increase from 4.0 to 4.5 MPa. The relative increment in the power

consumption of P1 is about 12.5%. Because the pump power is very small in

comparison with the expander output (about 1.5% of the latter) [15], the influence of

the pressure drop in the PTCs will be slight.

4.2.4. Thermal efficiency of the cascade Rankine cycle

Heat-to-power conversion efficiency of the SORC is

$$\eta_{SORC} = \frac{W_{net}}{m_1(h_1 - h_4)} \tag{14}$$

$$W_{net} = \left(W_{SE} + W_T\right) \cdot \varepsilon_g - \left(W_{p1} + W_{p2}\right) \tag{15}$$

Analogously, for the SRC and ORC,

$$\eta_{SRC} = \frac{W_{SE} \cdot \varepsilon_g - W_{p1}}{m_1(h_1 - h_4)} \tag{16}$$

$$\eta_{ORC} = \frac{W_T \cdot \varepsilon_g - W_{p2}}{m_{II}(h_5 - h_8)} \tag{17}$$

4.3. Solar thermal power generation efficiency

Thermal efficiency (η_T) of the proposed system indicates how effectively solar

radiation is converted into electricity.

$$\eta_T = \eta_{SORC} \cdot \eta_{PTC} = \frac{W_{net}}{G_b \cdot A} \tag{18}$$

4.4. Part-load behavior of SE

Built-in volume ratio of SE ($r_{v,b}$) is defined as

$$r_{v,b} = \frac{v_{out,b}}{v_{in,b}} \tag{19}$$

14

The operating pressure ratio (r_p) is defined as

$$r_p = \frac{p_{in}}{p_{out}} \tag{20}$$

$r_{v,b}$ and r_p are the known parameters normally available in the literature [45].

There are four types of losses in SE operation [38]:

(i)   Loss due to mismatch of the operating pressure ratio to the built-in $r_{p,b}$;

(ii)   Fluid leakage loss;

(iii)   Loss due to thermodynamic irreversibility;

(iv)   Mechanical friction loss from the rotating shaft.

For each stage of the work loss, an efficiency term can be specified to account for it. They are theoretical, leakage, thermodynamic and mechanical efficiencies for (i)-(iv), respectively. The actual overall isentropic efficiency can thus be defined as:

$$\varepsilon_{os} = \varepsilon_{Th}\varepsilon_L\varepsilon_{TM}\varepsilon_M = \varepsilon_{Th}\varepsilon_D\varepsilon_M \tag{21}$$

where
$$\varepsilon_D = \varepsilon_L\varepsilon_{TM} \tag{22}$$

ε_M is determined by the characteristic of SE, and it has a constant value for a specific SE. By definition, the theoretical efficiency is given as [38]:

$$\varepsilon_{Th} = \frac{W_{TD}}{W_{TI}} = \frac{(1 - r_{v,b}^{1-\gamma}) + (\gamma - 1)(1 - r_{v,b}/r_p)}{\gamma[1 - r_p^{(1-\gamma)/\gamma}]} \tag{23}$$

where W_{TD} and W_{TI} are theoretical diagram power and theoretical isentropic power respectively. γ is the isentropic index. It depends on the working fluid and its state and is 1.13 for dry saturated steam. 'Pseudo-polytropic' index could replace γ to give the actual expansion path of fluid when it is correlated against the specified inlet and outlet conditions [45].

The thermodynamic work output can be estimated by summing the shaft work output and the frictional work, i.e.

$$W_{TM} = W_S + W_F \qquad (24)$$

The actual W_{TM} could be well lower than the polytropic work output attributed to the irreversibility losses of fluid expansion and admission, blowdown exhaust and other leakage losses. W_F is a direct function of the shaft speed N. It is generally assumed to be unchanged if the rotation speed is held constant. Mechanical friction is insignificant as compared with the mismatching of r_p, leakage and presence of thermodynamic irreversibilities [45].

The diagram efficiency is given by the ratio of the thermodynamic work to the theoretical diagram work, i.e.

$$\varepsilon_D = \frac{W_{TM}}{W_{TD}} = \frac{W_S + W_F}{m_t p_{su} v_s \left[\frac{(1 - r_{v,b}^{1-\gamma})}{\gamma - 1} + (1 - \frac{r_{v,b}}{r_p}) \right]} \qquad (25)$$

The definition of diagram efficiency includes the effect of leakage and thermodynamic irreversibility. The leakage mass flow rate in an expander can be estimated using the ideal-gas choked flow model with a given leakage flow area [46]. Therefore, it is expected that the behavior of diagram efficiency is similar to that in the conventional turbomachines. Increment in $r_{v,b}$ has a negative effect on the diagram efficiency, but the efficiency variation is quite slight at high r_p [47].

Peak isentropic efficiency ($\varepsilon_{os,p}$) can be achieved when $\varepsilon_{Th,p}$ is 1.

$$\varepsilon_{os,p} = \varepsilon_{Th,p} \varepsilon_D \varepsilon_M \qquad (26)$$

Combine Eqs. (21), (23) and (26), ε_{os} can be estimated as:

$$\varepsilon_{os} = \varepsilon_{os,p}\varepsilon_{Th} = \varepsilon_{os,p} \cdot \frac{\varepsilon_D}{\varepsilon_{D,p}} \frac{(1 - r_{v,b}^{1-\gamma}) + (\gamma - 1)(1 - r_{v,b}/r_p)}{\gamma(1 - r_p^{1-\gamma/\gamma})} \qquad (27)$$

According to Eq. (27), the actual SE efficiency is affected by the operating r_p, $\varepsilon_{os,p}$, $r_{v,b}$, working fluid and state.

4.5. Cost of heat storage units

The thermodynamic performance comparison between the DSG and HTF systems can be made by the above models. Economic performance is important and a confrontation can be also conducted. According to Figs.1 and 2, costs of the heat storage units and collectors are the remarkable difference between the two types of systems. The collector cost can be figured out by the overall areas, which is related to the system power efficiency. Given a plant capacity, the cost of thermal energy storage (e.g. 6.5 hours) depends upon many factors involving the size of vessel, materials of construction, shape, welding requirements and additional custom standards. Taking into account all these factors will make the calculation difficult. However, like large heat exchangers whose cost is mainly contributed by the exchanger area and hence total amount of materials in use [48-49], large pressure vessels have the cost in approximate proportion to the vessel weight [50]. In particular, comparison between thermal storages using water and oil for the SE-based SEGS is one key issue in this work. The two fashions of storage units have similar cost related to indirect equipment expense, direct field labor for manufacture and installation, etc. The water-type storage is distinguishable from the other in view of the need of more steel for the vessel and the avoidance of expensive oil. Based on the above consideration, this section pays attention to the cost of materials for heat storage.

The material cost of steam accumulator is determined by

$$C_{s,DSG} = P_{steel}m_{steel} = P_{steel}\rho_{steel}V_{steel} \times 10^{-9} \qquad (28)$$

$C_{s,DSG}$ is the total cost. P_{steel} is the cost per kilogram. Alloy steel, stainless steel and carbon steel are favorable in pressure vessel applications. Cylinder vessel is commonly adopted. The total volume of steel (V_{steel}) is a function of the diameter (D_i), thickness (δ) and height (H) of the vessel. The design δ of the cylinder is correlated with the design pressure [51]

$$\delta_{cy} = \frac{pD_i}{2[\sigma]^t\phi - p} \qquad (29)$$

The units for pressure and diameter are MPa and mm, respectively. ϕ is the welding coefficient. $[\sigma]^t$ is the permissible stress.

The material mass used for the cylinder is

$$M_{steel,cy} = \rho_{steel}V_{steel,cy} \times 10^{-9} = \rho_{steel}\pi[(0.5D_i + \delta_{cy})^2 - 0.25D_i^2]H_{cy} \times 10^{-9} \qquad (30)$$

Cylinder vessel generally has two elliptical heads at the top and the bottom. The standard ratio of the half long axis (*a*) and the half short axis (*b*) of an ellipse is 2:1. The design thickness is expressed by

$$\delta_{head} = \frac{pD_i}{2[\sigma]^t\phi - 0.5p} \qquad (31)$$

The surface area (mm^2) and mass (kg) of an elliptical head are calculated by [52]

$$A_{head} = \pi a\{a + \frac{b}{\sqrt{(\frac{a}{b})^2 - 1}}\ln[\frac{a}{b} + \sqrt{(\frac{a}{b})^2 - 1}]\} + 2\pi ah_{head} \qquad (32)$$

$$M_{steel,head} = \rho_{steel}\pi\{[\frac{2}{3}(a + \delta_{head})^2(b + \delta_{head}) + (a + \delta_{head})^2 h_{head}] - (\frac{2}{3}a^2b + a^2h_{head})\} \times 10^{-9} \quad (33)$$

For a standard head as shown in Fig. 4, *a*=0.5*D*$_i$, *b*=0.5*a*.

$$A_{head} = 0.345\pi D_i^2 + \pi D_i h_{head} \tag{34}$$

$$M_{steel,head} = \rho_{steel}\pi\delta_{head}[\frac{D_i^2}{3} + \frac{5}{6}D_i\delta_{head} + \frac{2}{3}\delta_{head}^2 + (D_i + \delta_{head})h_{head}]\times10^{-9} \tag{35}$$

h_{head} can be 25, 40 and 50 mm as regulated by the standard [53].

The total mass of material used for the vessel is approximated by

$$M_{steel} = M_{steel,cy} + 2M_{steel,head} \tag{36}$$

The design pressure p is the sum of the saturation pressure (p_s) of water at the design temperature and the static pressure (p_g) caused by gravity. The vessel can be laid up in two ways (as shown in Fig. 5) determined by the axis of symmetry of the cylinder. For a vessel of vertical axis, the design pressure is expressed by

$$p = p_s + p_g = p_s + \rho_w g(H_{cy} + 2b + 2h_{head})\times10^{-9} \tag{37}$$

For a vessel of horizontal axis, the design pressure is expressed by

$$p = p_s + p_g = p_s + \rho_w g D_i \times10^{-9} \tag{38}$$

The determination of permissible stress is not at discretion. There are strict technical standards. Permissible stresses for six types of materials are listed in Table 1, which is guideline for the vessel design.

For the thermal oil storage unit,

$$C_{s,HTF} = C_{s,steel} + C_{s,oil} \tag{39}$$

$$C_{s,oil} = P_{oil}\rho_{oil}V_{oil} \tag{40}$$

$$\rho_{oil}V_{oil} = \frac{3600t_H \cdot W_{net}}{\eta_{SORC} \cdot C_{p,oil} \cdot \Delta T} \tag{41}$$

t_H is storage time in hour. $C_{p,oil}$ is the heat capacity of the oil. ΔT is the temperature drop from the hot to the cold tank.

5. Results and discussion

In this section, optimization of the SEGSs using water (direct system) and oil (indirect system) as heat transfer medium in the PTCs is first implemented at certain solar radiation and environment temperature. Mode 1 in Section 3 is exemplified. The objective function is solar electricity efficiency. The variables are SRC evaporation temperature (T_1) and ORC evaporation temperature (T_5), which may be deemed as two dimensional arrays $[T_1, T_5]$. After finding out the optimum $[T_{1,op}, T_{5,op}]$ on the given boundary conditions, cost-effectiveness of the thermal storage unit is investigated. Mass of steel at the preferable operation temperature is subsequently estimated in consideration of parametric distributions and arrangements of the vessels. Finally, cost comparison between DSG and HTF systems is conducted.

Some specific parameters and their values are listed in Table 2. R245fa is chosen for the ORC. Subcritical cycles are considered for both ORC and SRC. The ORC turbine has a constant efficiency.

5.1. The optimum hot side temperature ($T_{H,op}$)

5.1.1. $T_{H,op}$ at 750 W/m^2

Fig. 6 shows the heat collection efficiencies of direct and indirect systems and the cascade cycle efficiency varying with the hot side temperature T_H (i.e. temperature at the SE inlet, T_1) under the beam solar radiation of 750 W/m^2. The ORC evaporation temperature varies with T_H in order to promote the heat-to-power conversion efficiency. Water prior to the SE remains at saturation vapor state. The temperature difference between thermal oil inlet and outlet is 50 °C. Temperature interval of neighboring points of T_H in calculation is 10°C. The collector efficiencies

for both systems decline approximately linearly with the increment in T_H. The heat carried away by water is divided into two parts: latent heat and sensible heat. Due to the heat transfer irreversibility the average operating temperature of thermal oil is larger than the water's. Solar energy collection of the DSG system is more efficient by 4%-10%. This superiority gets more appreciable as T_H increases.

The power conversion efficiency of SORC first climbs when T_H rises, and then approaches to the peak point at T_H around 320 ℃, and drops with further temperature increment. It is not a monotonically increasing function of the hot side temperature, which is inconsistent with the behavior of a Rankine cycle of constant expander efficiency. There are two reasons behind this phenomenon. For subcritical ORC with working fluid of R245fa, the efficiency goes up insignificantly or even falls down as the evaporation temperature (T_5) moves close to its critical temperature (154 ℃), attributed to the decrement in the fluid's equivalent hot side temperature [55]. The other reason is that SE will go through highly off-design operation as T_H increases due to the small built-in volume ratio. The power conversion in the SRC suffers from the degraded SE performance.

The solar thermal electricity efficiencies of the DSG and indirect systems varying with T_H are depicted in Fig. 7. Both curves have parabola-like shapes, and open downward. At each T_H, the DSG system has a higher efficiency than the indirect one. The maximum efficiency is 14.3% and 13.2% for the former and the latter. And the corresponding optimum T_H is about 240 ℃ and 230 ℃. Given the solar radiation and ambient temperature, it can be deduced that the optimum T_H of the DSG system

surpasses that of the indirect system. According to Eq. (18), the derivative of solar electricity efficiency with respect to T_H is expressed as

$$\frac{d\eta_T}{dT_H} = \eta_{SORC}\frac{d\eta_{PTC}}{dT_H} + \eta_{PTC}\frac{d\eta_{SORC}}{dT_H} \tag{42}$$

When T_H is lower than 320 °C, $\frac{d\eta_{SORC}}{dT_H} > 0$ and $\frac{d\eta_{PTC}}{dT_H} < 0$. For common solar collectors, η_{PTC} and $\left|\frac{d\eta_{PTC}}{dT_H}\right|$ (absolute value) are monotonically decreasing and increasing functions of T_H, respectively. Given T_H, the expression for DSG system differs from the indirect system's in the collector efficiency ($\eta_{PTC,DSG}$ and $\eta_{PTC,HTF}$). The relationship between them is

$$\eta_{PTC,HTF}(T_H) \approx \eta_{PTC,DSG}(T_H + \alpha), \quad \alpha > 0 \tag{43}$$

For both systems, T_H at the peak efficiency points ($T_{H-DSG,op}$ and $T_{H-HTF,op}$) shall fulfill

$$\frac{d\eta_T}{dT_H} = 0 \tag{44}$$

$$\left.(\eta_{SORC}\frac{d\eta_{PTC,DSG}}{dT_H} + \eta_{PTC,DSG}\frac{d\eta_{SORC}}{dT_H})\right|_{T_H = T_{H-DSG,op}} = 0 \tag{45}$$

$$\left.(\eta_{SORC}\frac{d\eta_{PTC,HTF}}{dT_H} + \eta_{PTC,HTF}\frac{d\eta_{SORC}}{dT_H})\right|_{T_H = T_{H-HTF,op}} = 0 \tag{46}$$

Because

$$\eta_{PTC,DSG}(T_H) > \eta_{PTC,HTF}(T_H) \tag{47}$$

$$\left|\frac{d\eta_{PTC,DSG}}{dT_H}\right| < \left|\frac{d\eta_{PTC,HTF}}{dT_H}\right| \tag{48}$$

Therefore

$$(\eta_{SORC} \frac{d\eta_{PTC,HTF}}{dT_H} + \eta_{PTC,HTF} \frac{d\eta_{SORC}}{dT_H}) \bigg|_{T_H = T_{H-DSG,op}} < 0 \qquad (49)$$

$\left| \dfrac{d\eta_{PTC,HTF}}{dT_H} \right|$ and $\eta_{PTC,HTF}$ are monotonic functions of T_H. Combining (46) and (49),

$$T_{H-DSG,op} > T_{H-HTF,op} \qquad (50)$$

5.1.2. $T_{H,op}$ varying with solar radiation

The influence of solar radiation on $T_{H,op}$ is illustrated by Fig. 8. The corresponding solar electricity efficiency variations are exhibited in Fig. 9. In the normal radiation ranges from 600 W/m² to 900 W/m², $T_{H,op}$ of the DSG system varies from 220 °C to 250 °C. It is comparatively low for the thermal oil-connected system. The maximum η_T ascends as the radiation turns stronger, though the increment becomes less significant. The efficiency difference between the DSG and indirect systems is about 0.9-1.5%, and the largest occurs at the lowest radiation. The detailed parameters on the optimum conditions at three levels of radiation are posted in Tables 3 and 4. The corresponding thermodynamic state points are marked in Figs.1 and 2.

5.1.3. Annual $T_{H,op}$ in six areas

Solar radiation fluctuates from time to time in practice. The optimum operation of the SEGS is linked with the local meteorology. The recommended $T_{H,op}$ at the design condition in six areas of rich solar energy resource is provided in Table 5. Hourly weather data in a typical year are used [56]. $T_{H,op}$ changes with the location and ranges from 200 °C to 240 °C. In other areas of poorer solar energy, $T_{H,op}$ is expected to be lower. The relative increment of annual power output of the DSG system by that on the use of the indirect system is around 10%.

23

The above analysis indicates that owing to the compromise among solar energy collection, temperature difference driving the cycle and irreversibility of SE, the preferable $T_{H,op}$ shall go below 250 °C. It is a desirable thermodynamic result since common SEs operate at pressure up to 4 MPa and water can be selected for heat storage.

5.2. Parametric effect on steam accumulators in the DSG system

Q345R is exemplified. It is currently the most widely used material for manufacturing vessels and boilers in China. It has been permitted in ASME Code Case 2642 for the fabrication of pressure vessels without concern on the low stress conditions [57]. It is a typical low alloy steel, originated from three old steel grades of 16MnR, 16Mng and 19Mng. It has good mechanical properties of low phosphorus and sulfur contents. Small amounts of trace elements are allowed to be added to improve smelting and rolling processes. The regulated quality of components for Q345R is listed in Table 6 [58]. Design thickness of vessel made of Q345R on different conditions of temperature, pressure and diameter is indexed in Table 7.

Based on the thermodynamic results in Section 5.1, a design temperature of 250 °C for the steam accumulator is selected. The saturation pressure of water at this temperature is 3.98 MPa. The practical temperature/pressure could be lower than the design. The reference radiation is 750 W/m². The total mass of water in use varies with the temperature range of operation. A larger temperature drop of water during heat discharge will lead to a smaller accumulator. But as the temperature descends, the supply pressure for SE will be diminished, thus affecting the power conversion. The

curve in Fig. 7 shows that the DSG system efficiency almost keeps constant when T_H stays within the interval of (230 ℃, 250 ℃). Therefore, the temperature drop is assumed to be 20 ℃ in the heat release process. Given cascade cycle efficiency (η_{SORC}) of 23.5% at 240 ℃ and 6.5 h storage, a total volume of 1204 m³ of water for storage is required, as calculated in a similar way by Eq.(41).

5.2.1. Single pressure vessel

Fig. 10 shows material consumption (M_{steel}) and vessel design pressure (p) varying with the diameter (D_i) for the vertical vessel. M_{steel} first decreases drastically as D_i increases, reaching a minimum value of about 861.3 tons at D_i of 4600 mm and then climbs gradually with further increment in D_i. The decline of M_{steel} is attributed to a lower p when the vessel is enlarged. The vessel volume is constant and the height (H_{cy}) is linearly inversely proportional to the square of D_i. So the increment of D_i leads to reduced H_{cy} and p. The influence of D_i on p becomes unnoticeable in the low range of H_{cy}. At D_i =5000 mm, H_{cy} is about 61 m and the pressure due to gravity is about 0.6 MPa, which is around one-seventh of the saturation pressure of water at 250 ℃. In this situation, D_i has limited effect on the design pressure but much more appreciable one on the mass of Q345R for the heads. When D_i changes from 5000 mm to 9000 mm, the overall head mass ($2 \times M_{steel,head}$) goes up from 43.0 tons to 229.6 tons.

The effect of D_i on M_{steel} and H_{cy} in case of horizontal vessel is graphed by Fig. 11. H_{cy} is actually the vessel length rather than the height so the design pressure is a weak function of D_i. Unlike that of vertical vessel, M_{steel} rises in a monotonic

fashion. In light of Eq. (29), given p and the permissible stress, δ_{cy} is almost proportional to D_i. Because $M_{steel,cy} \approx \pi\rho_{steel}D_i\delta_{cy}H_{cy} \approx \pi\rho_{steel}D_i\delta_{cy}V_{vessel}/(0.25\pi D_i^2)$, so $M_{steel,cy} \propto \delta_{cy}/D_i$ and nearly unvaried $M_{steel,cy}$ can be expected. Meanwhile, higher D_i is accompanied by larger $M_{steel,head}$, resulting in a monotonically increasing M_{steel} with increment in D_i. Several sudden growths in M_{steel} are observed at D_i around 1100, 2300, 3500, 5400 and 7800 mm. They are caused by the non-continuous regulated permissible stress of Q345R. The stress may de-escalate abruptly as wall thickness increases. At each D_i, M_{steel} of the horizontal vessel gets below the vertical's. When D_i =4600 mm, the former is 735.5 tons, nearly 14.6% lower than the latter. The difference turns larger at smaller D_i.

Figs. 10 and 11 indicate D_i of no more than 5000 mm is material-saving. In particular, the horizontal vessel always benefits from the decrement in D_i in terms of the consumption of Q345R. However, H_{cy} could be extremely high at low D_i. It is about 72 m at D_i =4600 mm. There will be great difficulty in fabrication and transportation of such a vessel.

5.2.2. Vessels in parallel

To solve the problem of unusual H_{cy}, two or more vessels can be employed concurrently. Figs. 12 and 13 present the relationship between M_{steel} and the number of vessels (N) in use. The vessels of a given number are of the same dimension and design pressure, and work in parallel with each other. For all cases, H_{cy} is fixed at 25 m. M_{steel} is the total mass of the vessels. Obviously, M_{steel} together with D_i drops as more vessels are utilized. The sudden decrements are facilitated by the hopping

δ_{cy} that could come along with discontinuous permissible stress.

The variations of M_{steel} for the vertical and horizontal vessels are similar. The horizontal placement still has superiority in the material usage when multi-vessels are combined. The reduction of mass ranges from 38.7 tons to 41.7 tons when N is within 12. It seems horizontal vessels are more beneficial than vertical ones for the water storage of the DSG solar power generation system.

Though multi-vessels offer comparatively low steel material cost, there may be several disadvantages. As the number increases, the processing cost is supposed to rise. Besides, the heat loss from the vessels could be more remarkable. The total surface area (S_{cy}) of the cylinders is approximately proportional to $N^{0.5}$ because

$$S_{cy} \approx N \cdot \pi \cdot D_i \cdot H_{cy} \approx N \cdot \pi \cdot [V_{steel} / (0.25N\pi H_{cy})]^{0.5} \cdot H_{cy} = (4V_{steel} \cdot \pi \cdot H_{cy})^{0.5} \cdot N^{0.5} .$$ A larger S_{cy} may lead to more cost for thermal insulation.

Considering the above pros and cons, N of 6 seems to be acceptable. And M_{steel} is about 709 tons in the presence of horizontal vessels, with δ_{cy} of 54.8 mm and D_i of 3195 mm.

5.3. Parametric effect on thermal oil storage

The two-tank system of oil or molten salt is the most proven utility-scale thermal storage system, and has been used or projected in many CSP plants including SEGS Ⅰ, the 10 MW Solar Two plant, the Andasol plant (1-3, 50 MW per plant) and the 280 MW Solana plant. The temperature range in which the storage unit is operated needs to be determined at its design stage. If the temperature difference between the hot and the cold tanks (ΔT) is broadened, more heat will be released during the discharge

process at a given tank size. Putting it differently, the tank size will be reduced with a widened temperature range at the given power output and capacity factor.

However, on the same conditions of T_H and pinch point temperature and solar radiation, the increment in ΔT elevates the hot tank temperature and effectuates lower efficiencies of heat collection and solar thermal power generation. The maximum η_T at different ΔT is displayed in Table 8. It declines monotonically as ΔT grows, which may lengthen the payback period of the SEGS. Moreover, as the operating temperature rises, the requirement on thermal and chemical stability of oil becomes stricter. And fewer sorts of oils will be applicable. An appropriate ΔT shall be the trade-off among the amount of oil, its applicability and system efficiency. In SEGS Ⅰ, ΔT was designed at 67 ℃ [18].

5.4. Cost comparison between water-based and oil-based storage technologies

According to the information of one of the pacesetting pioneers in China's steel E-Commerce sector, the current market price of Q345R ranges from 3000 RMB to 4200 RMB per ton [59]. Thermal oils which have been employed in PTC-CSP plants such as Therminol VP-1 [60], ENE L-QB300 and ENE L-QD400 [61] cost about 12000-25000 RMB per ton. In the following comparison, the prices of Q345R and thermal oil are assumed to be 3600 and 18500 RMB per ton, respectively.

The cost variation of thermal oil with ΔT is exhibited in Fig. 14. The cost of Q345R is also referenced. It is about 2.55 million RMB given ΔT of 20 ℃ and total mass of 709 tons, which remains constant in the chart. For the oil, the cost decreases with the increment in ΔT. The decrement is not linear owing to the diversified

electricity efficiency. At $\Delta T = 100\,^{\circ}C$, the oil cost is 7.92 million RMB with a mass of 428.2 tons. The cost superiority of steam accumulator over thermal oil storage is evident. It is noteworthy that oil needs to be periodically replaced or reprocessed. Its lifetime is about 5 years, more or less.

The results indicate water as the thermal storage, heat transfer and working fluid of the SE-based SEGS is feasible. Supported by the data, it is not complicated to find out the reason why the steam accumulator does not has so good applicability in the conventional turbine-driven SEGS as in the proposed system. First, the design pressure is much larger. As pointed out by predecessors, a main steam condition of $500\,^{\circ}C$ /12 MPa could provide lower LCOE for the PTC-DSG power plant than those of $400\,^{\circ}C$ /12 MPa and $500\,^{\circ}C$ /10 MPa [62]. In this case, the design pressure is 3 times of 4 MPa. Second, the design temperature is higher. The permissible stress of material generally drops as the operating temperature increases. For example, it is about 130 MPa -167 MPa for Q345R at $250\,^{\circ}C$, and becomes merely 66 MPa at 450 $^{\circ}C$. Third, the material gets limited. At temperature above $500\,^{\circ}C$, Q345R, Q245R, etc. are not competent. 15CrMoR could be an alternative, but its price is almost twice of Q345R [63]. Fourth, the accumulator shall be much thicker. Since δ_{cy} and δ_{head} are approximately proportional to the design pressure and permissible stress, they may be 6 times thicker than those in the SE-related system. The permissible stress will be further degraded at the same design temperature and pressure as it is a thickness-dependent parameter. Counting on these issues, the cost of steam accumulator for the traditional SEGS operating at high temperature and pressure is

supposed to transcend that of thermal oil.

5.5. Uncertainty analysis

Thermodynamic performances of the DSG and indirect systems are sensitive to efficiencies of the PTCs, SE and ORC turbine. The deployed PTCs have optical efficiency of 0.762, first and second loss coefficients of 0.2125 $W/(m^2K)$ and 0.001672 $W/(m^2K^2)$. The collector efficiency is about 0.585 with solar radiation of 750W/m^2 and operating temperature of 250 °C, which is lower than those of products such as Schott LS-2 [64] and Eurotrough 150 [65]. The SE and ORC turbine have a design efficiency of 0.75. Isentropic efficiency of around 0.72 for small SE (10-50kW) has been experimentally reported [66-67]. For large SEs, efficiency approaching 0.80 can be expected [68]. The turbine-based ORC is mature nowadays with installation capacity more than 1.8 GW [69]. Turbine efficiency above 0.8 is common [70-71]. Constant turbine efficiency is assumed in the optimization. In comparison with SE, turbine can be designed at a much higher expansion ratio. Nominal efficiency over 0.8 for single-stage axial turbine is expected when the built-in expansion ratio is below 50 [72]. From Table 3, the expansion ratio of R245fa on a recommended working condition is about 12. Even if the ORC evaporation temperature increases to 140 °C, the ratio will remain less than 16. Once the optimum working condition is determined, it is easy to design the turbo-expander accordingly. Besides, multi-stage turbine is popular for high expansion ratio applications.

Therefore, device efficiencies in the simulation are reasonable and the thermodynamic performance of the proposed SGES does not seem to be

over-estimated. The PTC, SE and ORC turbine are the same in DSG and indirect systems, if they are replaced the efficiency superiority of the DSG system shall be retained.

Cost comparison between the DSG and indirect systems are made on the conditions of thermal storage of 6.5 hours, steel and oil prices of 3600 RMB and 18500 RMB respectively. The prices of steel and oil may change with time. The storage cost ($C_{p,steel}$, $C_{p,oil}$) can be simply deduced because there is a linear relationship between $C_{p,steel}$, $C_{p,oil}$ and the material price. $C_{p,steel}$ and $C_{p,oil}$ are also proportional to the storage time.

In the comparison, cascade cycle efficiency (η_{SORC}) of the DSG system of 23.5% is employed. However, heat charging and discharging lead to temperature fluctuation in the accumulator and the power conversion is not steady. The variation of η_{SORC} during the unsteady process is shown in Fig. 15. The design T_H is 240 °C. η_{SORC} increases with the increment in the accumulator temperature. The deviation from the design is within (-0.45%, +0.35%), which is slight. Variation of the equivalent solar thermal electricity efficiency (η_T) is also depicted in the figure. When heat is released due to an accumulator temperature decrement from ($T + \Delta T$) to T, equal energy should be harvested from the solar field in the periodical operation. So the equivalent η_T is deemed as the product of η_{SORC} and η_{PTC} at T. Deviation of η_T falls within an interval of (-0.09%, +0.01%).

6. Conclusion

The SE-based DSG solar thermal electricity system using cascade Rankine cycle is

designed. The principle is illustrated. By establishing the part-load model on the SE, a close view to the performance of the proposed system can be brought and parametrical optimization can be executed. Thermo-economic comparison between the DSG and indirect systems is made, followed by further discussion on the uncertainty.

Maximum solar thermal electricity efficiency ($\eta_{T,m}$) and optimum hot side temperature of the SORC ($T_{H,op}$) are 14.3% and 240 °C respectively under beam solar radiation of 750 W/m² for the DSG SGES. There are deviations of (-0.9%, +0.6%) in $\eta_{T,m}$ and (-20 °C, +10 °C) in $T_{H,op}$ when the radiation range is widened from 600 W/m² to 900 W/m². $T_{H,op}$ for system's annual operation in six territories of abundant solar energy resource i.e. Phoenix, Sacramento, Cape Town, Canberra, Barcelona and Lhasa falls within (220 °C, 240 °C).

Replacing the DSG solar field by collectors working with thermal oil, both $\eta_{T,m}$ and $T_{H,op}$ are decreased on the same conditions of solar radiation and environment temperature. The decrement in $\eta_{T,m}$ is about 1.1% at 750 W/m², which turns more appreciable at lower radiation. And the annual electricity generation suffers from a yield drop around 10% in the six areas.

Aside from the thermodynamic benefits, the DSG system has cost advantage over the indirect one in terms of storage. The concept of using steam accumulators for heat storage in DSG plant has been discussed in the literatures. In this work, mathematical model is built and the material cost of the accumulators is analyzed in detail at an eligible design temperature of 250 °C. The horizontal pressure vessels appear to save

more material of steel than the vertical ones. And the total occupied mass tends to decrease with the decrement in the vessel diameter. Multi-vessels functioning in parallel can effectively reduce the device length. When 6 vessels of length of 25 m are used and a temperature drop of 20 ^{o}C during heat discharge (ΔT) is assumed, an amount of 709 tons of Q345R is needed for 6.5 h storage in a 1 MW plant.

To facilitate a similar storage using the two-tank HTF system, the required oil is 428.2 tons on the assumption of $\Delta T = 100$ ^{o}C. In accordance with the current market price, the thermal oil cost is three times more than that of the steel material for steam accumulators.

Reference

[1] Opcon Powerbox Product Sheet.

<http://opconenergysystem.com/en/opcon-powerbox-wst-cu/> [06.08.16].

[2] Why Heliex. <www.heliexpower.com/why-heliex/whats-required/> [20.08.16].

[3] Parameters & Specifications.

<http://www.jxhdep.com/newsInfo.asp?pid=88&small=89&id=237> [25.08.16].

[4] Specifications. <http://qyexpander.com/chanpin.htm> [14.08.16].

[5] The Power+ 6500 comes in two configurations – Stand alone or turnkey package. <https://electratherm.com/products/power-plus-generator-6500-up-to-110kwe> [31.01.17].

[6] ORC Screw Expansion Power Station. <http://www.denair.net/ORC/ORC_screw_expansion_power_station.html> [30.01.17].

[7] Zhai H, Dai YJ, Wu JY, Wang RZ. Energy and exergy analyses on a novel hybrid solar heating, cooling and power generation system for remote areas. Appl Energy 2009; 86: 1395-404.

[8] Astolfi M. Techno-economic optimization of low temperature CSP systems based on ORC with screw expanders. Energy Procedia 2015; 69: 1100-12.

[9] Joung J, Cho H. Theoretical analysis of a small-scale solar power system using an R-245fa Rankine cycle with a scroll and twin screw expander. WIT Transactions on Ecology and The Environment 2015; ISSN 1743-3541: 206-17.

[10] CLEAN ELECTRICITY FROM WET STEAM. <http://www.rushlightevents.com/wp-content/uploads/2014/01/R-Show-14-SSMP-Heliex-Power.pdf> Heliex Power Ltd. [31.01.17].

[11] Merigoux JM, Pocard P. Solar power units with screw expanders. In: Solar energy: International progress; Proceedings of the International Symposium-Workshop, Cairo, Egypt, June 16-22, 1978. vol. 3. New York, Pergamon Press, Inc., 1980, p. 1293-317.

[12] Song J, Gu CW. Performance analysis of a dual-loop organic Rankine cycle (ORC) system with wet steam expansion for engine waste heat recovery. Appl Energy 2015; 156: 280-9.

[13] Tang Y. Single stage and cascaded organic Rankine cycles with screw expanders used for hot fluids in oil refineries and chemical plants. 16th International Refrigeration and Air Conditioning Conference at Purdue, July 11-14, 2016.

[14] Zhang HG, Wang EH, Fan BY. A performance analysis of a novel system of a dual loop bottoming organic Rankine cycle (ORC) with a light-duty diesel engine. Appl Energy 2013; 102: 1504-13.

[15] Li J, Li PC, Pei G, Alvi JZ, Ji J. Analysis of a novel solar electricity generation system using cascade Rankine cycle and steam screw expander. Appl Energy 2016; 165: 627-38.

[16] James E, Pacheco. Demonstration of solar-generated electricity on demand: the solar two project. J. Sol. Energy Eng-Transactions of the ASME 2001; 123: 5.

[17] Medrano M, Gil A, Martorell I, Potau X, Cabeza LF. State of the art on high-temperature thermal energy storage for power generation. Part 2-Case studies. Renewable & Sustainable Energy Reviews 2010; 14: 56-72.

[18] Solar Electric Generating Station I.

<http://www.nrel.gov/csp/solarpaces/project_detail.cfm/projectID=28> [13.09.16].

[19] Huang SY, Huang SH. Solar thermal power generation principle and technology. China Electric Power Press, Chapter Ten 2012: 446.

[20] Laing D, Bahl D, Bauer T, Lehmann D, Steinmann WD. Thermal energy storage

for direct steam generation. Sol Energy 2011; 85: 627-33.

[21] Birnbaum J, Eck M, Fichtner M, Hirsch T, Lehmann D, Zimmermann G. A direct steam generation solar power plant with integrated thermal storage. 14th Biennial CSP SolarPACES (Solar Power and Chemical Energy Systems) Symposium, Las Vegas, USA, NREL/CD-550-42709; 2008.

[22] Bai FW, Xu C. Performance analysis of a two-stage thermal energy storage system using concrete and steam accumulator. Appl Therm Eng 2011; 31: 2764-71.

[23] Garcia1 P, Vuillerme V, Olcese M, Mourchid NE. Design and modelling of an innovative three-stage thermal storage system for direct steam generation CSP plants. AIP Conf. Proc 2016; 1734: 050015.

[24] Steinmann WD, Eck M. Buffer storage for direct steam generation. Sol Energy 2006; 80: 1277-82.

[25] SOLUCAR. PS10: 10 MW solar thermal power plant for southern Spain. NNE5-1999-356; 2016.

[26] Planta Solar 20. National Renewable Energy Laboratory.
<http://www.nrel.gov/csp/solarpaces/project_detail.cfm/projectID=39> [22.06.16].

[27] Feldhoff JF, Schmitz K, Eck M, Schnatbaum-Laumann L, Laing D, Ortiz-Vives F, Schulte-Fischedick J. Comparative system analysis of direct steam generation and synthetic oil parabolic trough power plants with integrated thermal storage. Sol Energy 2012; 86: 520-30.

[28] Ruiz-Cabañas FJ, Prieto C, Osuna R, Madina V, Fernández AI, Cabeza LF. Corrosion testing device for in-situ corrosion characterization in operational molten

salts storage tanks: A516 Gr70 carbon steel performance under molten salts exposure. Sol. Energ. Mater. Sol. Cells 2016; 157: 383-92.

[29] Sau S, Corsaro N, Crescenzi T, D'Ottavi C, Liberatore R, Licoccia S, Russo V, Tarquini P, Tizzoni AC. Techno-economic comparison between CSP plants presenting two different heat transfer fluids. Appl Energy 2016; 15: 96-109.

[30] Srivastava AK, Kudariyawar JY, Borgohain A, Jana SS, Maheshwari NK, Vijayan PK. Experimental and theoretical studies on the natural circulation behavior of molten salt loop. Appl Therm Eng 2016; 98: 513-21.

[31] Dorcheh AS, Galetz MC. Slurry aluminizing: A solution for molten nitrate salt corrosion in concentrated solar power plants. Sol. Energ. Mater. Sol. Cells 2016; 146: 8-15.

[32] Myers Jr PD. Alamb TE, Kamal R, Goswami DY, Stefanakos E. Nitrate salts doped with CuO nanoparticles for thermal energy storage with improved heat transfer. Appl Energy 2016; 165: 225-33.

[33] Vignarooban K, Xu X, Wang K, Molina EE, Lic P, Gervasio D, Kannan AM. Vapor pressure and corrosivity of ternary metal-chloride molten-salt based heat transfer fluids for use in concentrating solar power systems. Appl Energy 2015; 159: 206-13.

[34] Smith IK, Stosic N, Kovacevic A. Screw expanders increase output and decrease the cost of geothermal binary power plant systems. Transactions of Geothermal Resource 2005.

[35] Papes I, Degroote J, Vierendeels J. New insights in twin screw expander

performance for small scale ORC systems from 3D CFD analysis. Appl Therm Eng 2015; 91: 535-46.

[36] Read M, Stosic N, Smith IK. Optimization of screw expanders for power recovery from low-grade heat sources. Energy Technol Policy 2014; 1: 131-42.

[37] Invernizzi C, Iora P, Silva P. Bottoming micro-Rankine cycles for micro-gas turbines. Appl Therm Eng 2007; 27: 100-10.

[38] Ng KC, Bong TY, Lim TB. A thermodynamic model for the analysis of screw expander performance. Heat Recov Syst CHP 1990; 10: 119-33.

[39] Li J, Pei G, Li YZ, Wang DY, Ji J. Energetic and exergetic investigation of an organic Rankine cycle at different heat source temperatures. Energy 2012; 38: 85-95.

[40] Nag HPK. Power Plant Engineering. Tata McGraw-Hill Education 2008 ISBN: 0070648158: 107.

[41] Cascade refrigeration stem. <http://www.nissin-ref.co.jp/english/product_blog/1-2.html> [20.01.17].

[42] Eck M, Hennecke K. Heat transfer fluids for future parabolic trough solar thermal power plants. Proceedings of ISES Solar World Congress 2007: Solar Energy and Human Settlement.

[43] Kruger D, Heller A, Hennecke K, Duer K. Parabolic trough collectors for district heating systems at high latitudes: a case study. Proceedings of Eurosun 2000.

[44] Soteris A. Kalogirou. Solar thermal collectors and applications. Progress in energy and combustion science 2004; 30: 231-95.

[45] Ng KC, Lira TB, Bong TY. Analysis of screw expander performance. Proc.

Insm Mechn. Engrs Part E 1989; 203: 15-20.

[46] Gordon FC, Rogers, Mayhew YR. Engineering Thermodynamics—Heat and Work Transfer. ELBS Book 1964.

[47] Koto-Ku B. Screw type steam engine. Internal report of Mayekawa Mfg Co Ltd, Japan 1984; 2-3-1: Tokyo 135.

[48] Hettiarachchi HDM, Golubovic M, Worek WM, Ikegami Y. Optimum design criteria for an Organic Rankine cycle using low-temperature geothermal heat sources. Energy 2007; 32: 1698-706.

[49] Cataldo F, Mastrullo R, Mauro AW, Vanoli GP. Fluid selection of organic Rankine cycle for low-temperature waste heat recovery based on thermal optimization. Energy 2014;72: 159-67.

[50] Vessel Cost Estimate. <http://matche.com/equipcost/Vessel.html> [26.07.16].

[51] Steel pressure vessels. National Standard of the People's Republic of China. GB 150-1998, pp:28.

[52] Heads for pressure vessels. National Standard of the People's Republic of China. GB/T 25198-2010, pp:13。

[53] Elliptical heads. Standards of the Machinery Department of the People's Republic of China. JB1154-73.

[54] Steel plates for boilers and pressure vessels. National Standard of the People's Republic of China. GB 713-2008.

[55] Li J, Alvi JZ, Pei G, Su YH, Li PC, Gao GT, Ji J. Modelling of organic Rankine cycle efficiency with respect to the equivalent hot side temperature. Energy 2016; 115：

668-83.

[56] Weather Data. <https://energyplus.net/weather> Energyplus [12.04.16]

[57] ASME, ASME Boiler & Pressure Vessel Code Case 2642, American Society of Mechanical Engineers, New York 2010.

[58] Steel plates for boilers and pressure vessels. National Standard of the People's Republic of China. GB 713-2014.

[59] FOB prices of steel products. <http://www.mysteel.net/> Shanghai Ganglian E-Commerce Co., Ltd. [25.9.16].

[60] THERMINOL® P-1. <http://www.szsolutia.com/productse_detail/id/7.html> Solutia Therminol Co. Ltd., Suzhou. [25.9.16].

[61] ENE L-QD400. <http://www.enesoon.com.cn/en/> Enesoon. [25.9.16].

[62] Feldhoff JF, Benitez D, Eck M, Riffelmann KJ. Economic potential of solar thermal power plants with direct steam generation compared with HTF plants. J Solar Energy Eng 2010; 132: 041001.

[63] FOB prices of steel products. <http://www.mysteel.net/> Shanghai Ganglian E-Commerce Co., Ltd. [25.9.16].

[64] Moss TA, Brosseau DA. Final Test Results for the Schott HCE on a LS-2 Collector. SANDIA REPORT. July 2005. SAND 2005-4034.

[65] Geyer M, Lerchenmüller H, Wittwer V, Häberle A, Lüpfert E, Hennecke K, Schiel W, Brakmann G: Parabolic trough system. FVS Themen 2002.

[66] Hsu SW, Chiang HWD, Yen CY. Experimental investigation of the performance of a hermetic screw-expander organic Rankine cycle. Energies 2014; 7: 6172-85.

[67] Avadhanula VK, Lin CS. Empirical models for a screw expander based on experimental data from organic Rankine cycle system testing. J Eng Gas Turbines Power 2014; 136: 062601-1.

[68] Smith IK. Review of the development of two-phase screw expanders. Progress in the Development of Twin Screw Machines. <http://www.staff.city.ac.uk/~sj376/smith99.htm> [01.02.17].

[69] Li J. Structural optimization and experimental investigation of the organic Rankine cycle for solar thermal power generation. Thesis, Springer 2015; ISBN 978-662-45622.

[70] Biomass cogeneration. Turboden <http://www.turboden.eu/en/applications/applications-biomass.php> [01.02.17].

[71] Sauret E, Gu YT. Three-dimensional off-design numerical analysis of an organic Rankine cycle radial-inflow turbine. Appl Energy 2014; 135: 202-11.

[72] Shu G, Li X, Tian H, Liang X, Wei H, Wang X. Alkanes as working fluids for high-temperature exhaust heat recovery of diesel engine using organic Rankine cycle. Applied Energy 2014; 119: 204-17.
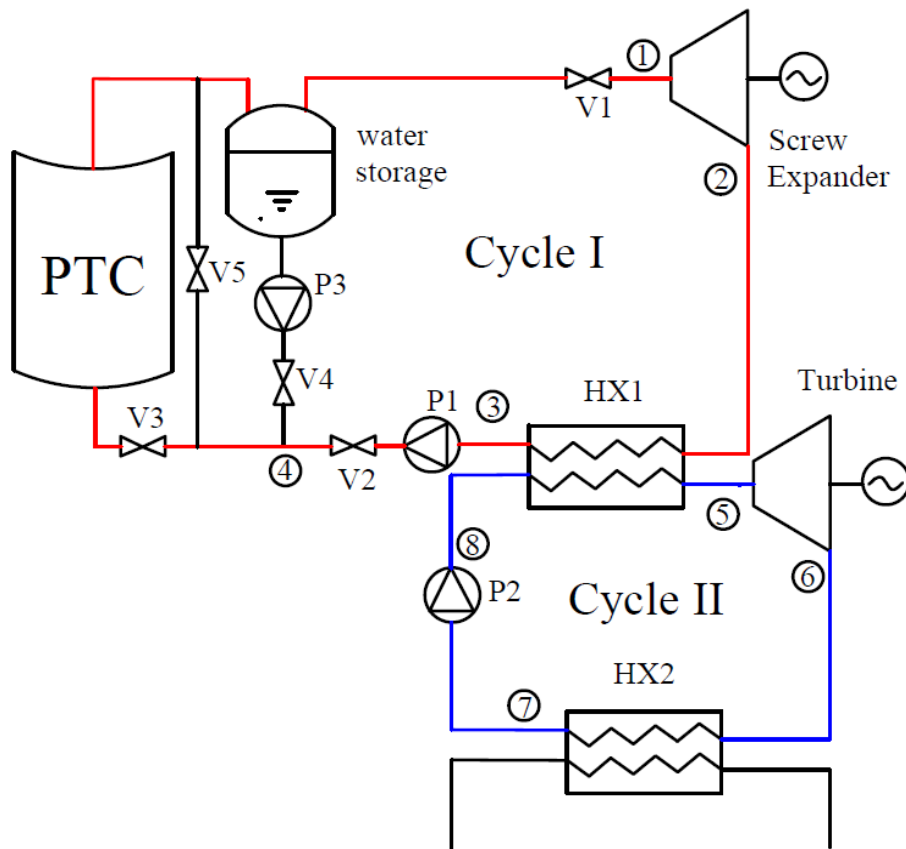
Figure Legends

Fig. 1. DSG solar cascade Rankine cycle system

Fig. 2. Solar cascade Rankine cycle system with thermal oil

Fig.3. T-s diagram of the cascade cycle

Fig. 4. Cross-section of elliptical head

Fig. 5. Different placements of pressure vessel

Fig. 6. Variations of the collector and cascade cycle efficiencies with the hot side temperature

Fig. 7. Variations of solar thermal power efficiencies with the hot side temperature

Fig. 8. Variation of the optimum hot side temperature with radiation

Fig. 9. Variation of maximum solar thermal power efficiency with radiation

Fig. 10. Variations of total mass and design pressure of Q345R with the diameter of vessel of vertical symmetrical axis

Fig. 11. Variations of total mass and length of the vessel of horizontal symmetrical axis with the diameter

Fig. 12. Variations of the total mass and the diameter with number of vessels in use for vertical placement

Fig. 13. Variations of the total mass and the diameter with number of vessels in use for horizontal placement

Fig. 14. Cost comparison between thermal oil and Q345R

Fig. 15. Variations of the cascade cycle efficiency and equivalent solar thermal power efficiency with the accumulator temperature in the heat charging/discharging process

Table Legends

Table 1. Permissible stress for some materials

Table 2. Fixed parameters

Table 3. Parameter distribution of the DSG system when maximum solar thermal power efficiency is achieved

Table 4. Parameter distribution of the indirect system when maximum solar thermal

power efficiency is achieved

Table 5. Optimum T_H and maximum power output in six regions

Table 6. Quality of different components for Q345R, unit: %.

Table 7. Design thickness under different working conditions for Q345R, unit: mm

Table 8. Maximum thermal power efficiency at different temperature drops from the

hot to the cold tank

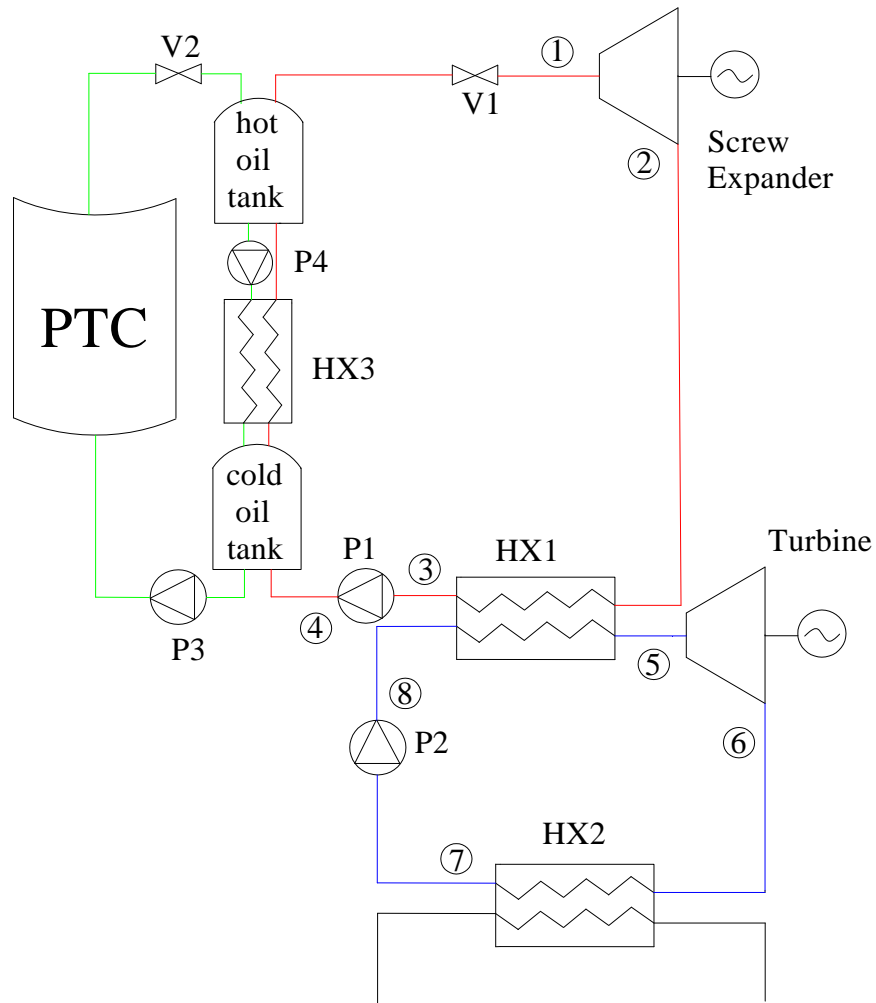Fig. 1. DSG solar cascade Rankine cycle system

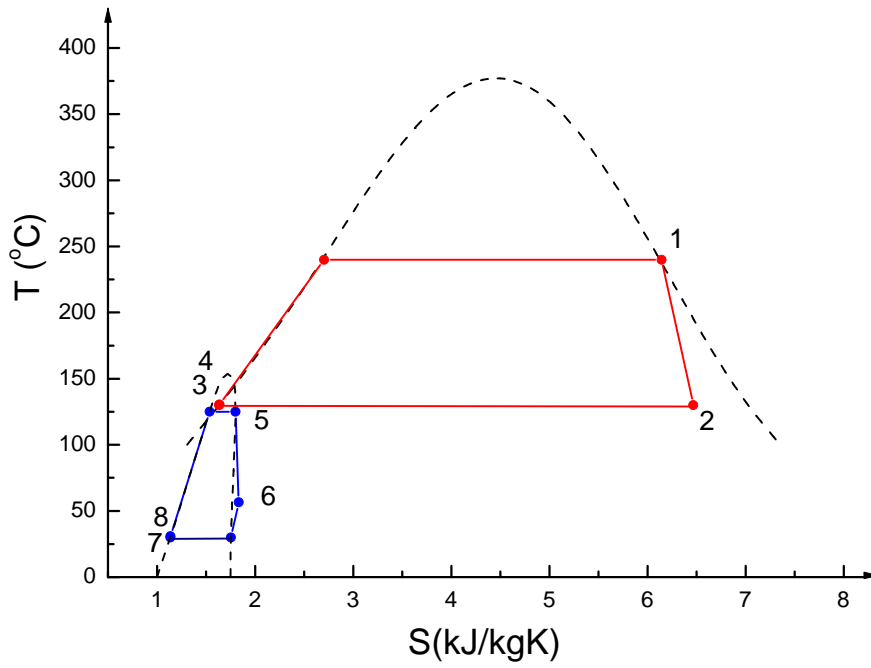Fig. 2. Solar cascade Rankine cycle system with thermal oil

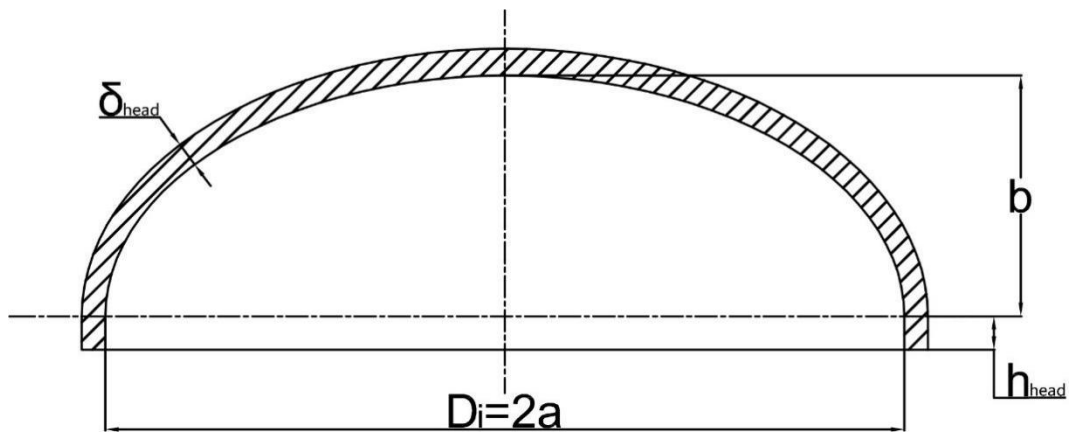Fig.3. T-s diagram of the cascade cycle

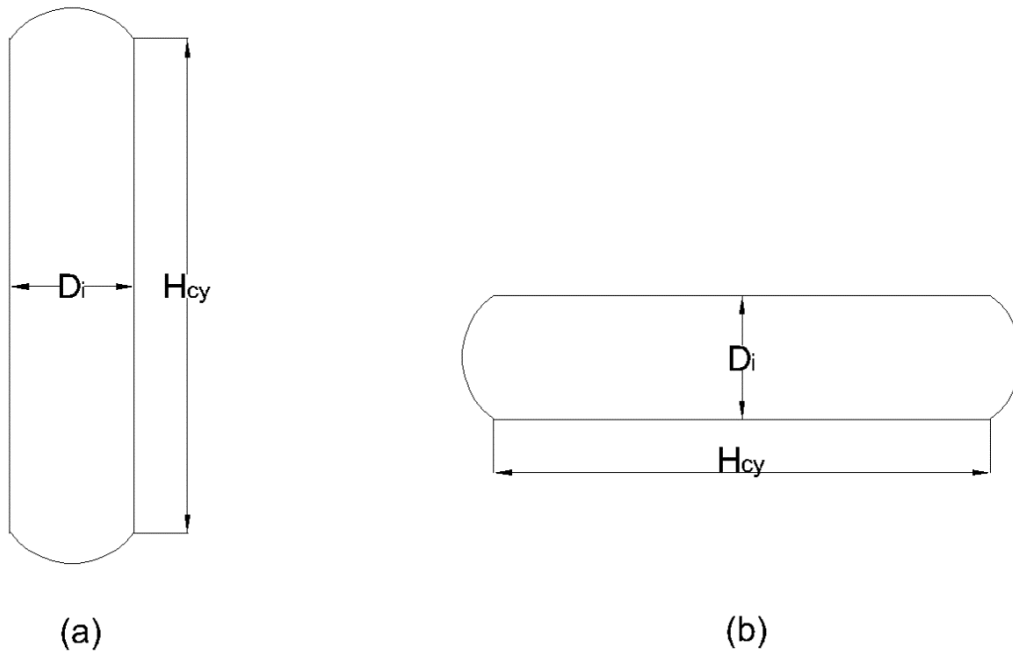Fig. 4. Cross-section of elliptical head

Fig. 5. Different placements of pressure vessel: (a) vertical; (b) horizontal

Fig. 6. Variations of the collector and cascade cycle efficiencies with the hot side

temperature

Fig. 7. Variations of solar thermal power efficiencies with the hot side temperature

Fig. 8. Variation of the optimum hot side temperature with radiation

Fig. 9. Variation of maximum solar thermal power efficiency with radiation

Fig. 10. Variations of total mass and design pressure of Q345R with the diameter of

vessel of vertical symmetrical axis

Fig. 11. Variations of total mass and length of the vessel of horizontal symmetrical

axis with the diameter

Fig. 12. Variations of the total mass and the diameter with number of vessels in use

for vertical placement

49

Fig. 13. Variations of the total mass and the diameter with number of vessels in use

for horizontal placement

Fig. 14. Cost comparison between thermal oil and Q345R

Fig. 15. Variations of the cascade cycle efficiency and equivalent solar thermal power

efficiency with the accumulator temperature in the heat charging/discharging process

Table 1. Permissible stress for some materials [54], unit: MPa

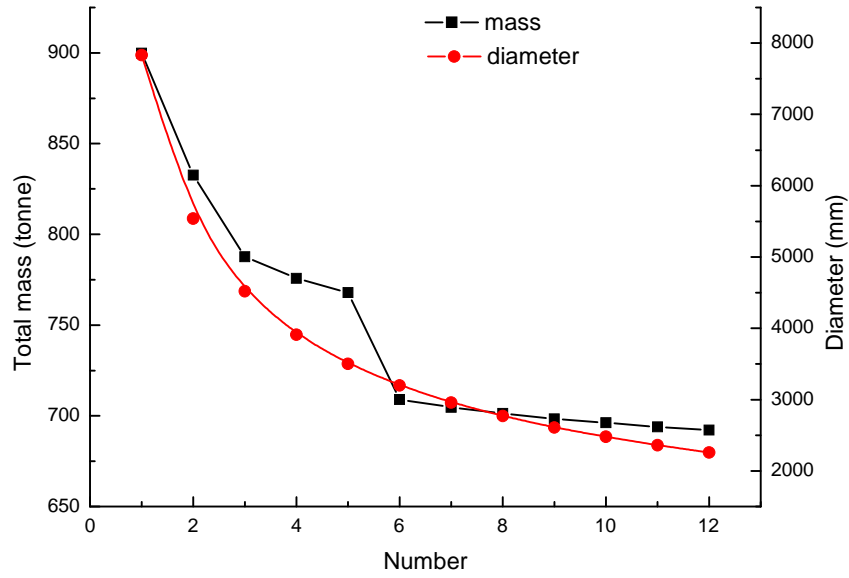| Type	Standard	Thickness /mm	Temperature / °C					
			200	250	300	350	400	450
Q245R	GB 713	3-16	131	117	108	98	91	61
		>16-36	124	111	102	93	86	61
		>36-60	119	107	98	89	82	61
		>60-100	109	98	90	82	75	61
		>10-150	100	90	80	73	70	61
Q345R	GB 713	3-16	183	167	153	143	125	66
		>16-36	170	157	143	133	125	66
		>36-60	160	147	133	123	117	66
		>60-100	150	137	123	117	110	66
		>100-150	147	133	120	113	107	66
		>150-200	143	130	117	110	103	66
15CrMoR	GB 713	6-60	160	150	140	133	126	119
		>60-100	147	140	131	124	117	111
		>100-150	140	133	123	117	110	104
Q370R		10~16	196	190	180	170		
		>16~36	193	183	173	163		
		>36~60	180	170	160	150		
16MnDR	GB 3531	6-16	167	153	140	130		
		>16-36	157	143	130	120		
		>36-60	150	137	123	117		
		>60-100	147	133	120	113		
		>100-120	143	130	117	110		
09MnNiDR	GB 3531	6-16	160	153	147	137		
		>16-36	150	143	137	127		
		>36-60	143	137	130	120		
		>60-120	140	133	127	117		

Table 2. Fixed parameters

Term	Value
Pinch-point temperature difference, T_{pp}	5 K
Pump efficiency, ε_p	0.8
Peak isentropic efficiency of SE, $\varepsilon_{os,p}$	0.75
Turbine isentropic efficiency, ε_T	0.75
Generator efficiency, ε_g	0.95
Built-in volume ratio of SE, $r_{v,b}$	5
Ambient temperature, T_a	25
Welding coefficient, ϕ	0.8
Gravity, g	9.8 m/s^2
Net power output, W_{net}	1 MW
Capacity of heat storage, t_H	6.5 hours

Table 3. Parameter distribution of the DSG system when maximum solar thermal

power efficiency is achieved

G_b (W/m^2)	600	750	900
T_1(°C) / P_1(MPa)	220 / 2.32	240 / 3.35	250 / 3.98
T_2(°C) / P_2(MPa)	121 / 0.21	130 / 0.27	134 / 0.30
T_3(°C) / P_3(MPa)	121 / 0.21	130 / 0.27	134 / 0.30
T_4(°C) / P_4(MPa)	121.31 / 2.32	130.47 / 3.35	134.58 / 3.98
T_5(°C) / P_5(MPa)	116 / 1.78	125 / 2.13	129 / 2.30
T_6(°C) / P_6(MPa)	55.22 / 0.18	56.58 / 0.18	56.89 / 0.18
T_7(°C) / P_7(MPa)	30 / 0.18	30 / 0.18	30 / 0.18
T_8(°C) / P_8(MPa)	30.81 / 1.78	30.99 / 2.13	31.07 / 2.30
η_T (%)	13.38	14.24	14.90

Table 4. Parameter distribution of the indirect system when maximum solar thermal

power efficiency is achieved

G_b (W/m^2)	600	750	900
T$_1$(°C) / P$_1$(MPa)	210 / 1.91	230 / 2.80	240 / 3.35
T$_2$(°C) / P$_2$(MPa)	114 / 0.16	126 / 0.24	130 / 0.27
T$_3$(°C) / P$_3$(MPa)	114 / 0.16	126 / 0.24	130 / 0.27
T$_4$(°C) / P$_4$(MPa)	114.25 / 1.91	126.39 / 2.80	130.47 / 3.35
T$_5$(°C) / P$_5$(MPa)	109 / 1.54	121 / 1.97	125 / 2.13
T$_6$(°C) / P$_6$(MPa)	53.70 / 0.18	56.09 / 0.18	56.58 / 0.18
T$_7$(°C) / P$_7$(MPa)	30 / 0.18	30 / 0.18	30 / 0.18
T$_8$(°C) / P$_8$(MPa)	30.69 / 1.54	30.90 / 1.97	30.99 / 2.13
η_T (%)	12.25	13.23	13.99

Table 5. Optimum T_H and maximum power output in six regions

Region	DSG system		Indirect system	
	Optimum T_H (°C)	Maximum power output (kWh·m⁻²·year⁻¹)	Optimum T_H (°C)	Maximum power output (kWh·m⁻²·year⁻¹)
Phoenix	240	351.16	220	322.33
Sacramento	240	294.99	220	270.46
Cape Town	230	252.78	210	230.75
Canberra	220	227.50	200	209.89
Barcelona	210	206.46	200	186.73
Lhasa	200	214.87	190	193.03

Table 6. Quality of different components for Q345R [58], unit: %

Component	value	Component	value	Component	value
C	≤0.20	Si	≤0.55	Cu	≤0.30
Ni	≤0.30	Cr	≤0.30	Mo	≤0.08
Nb	≤0.05	V	≤0.05	Ti	≤0.03
Alt	>0.02	P	≤0.025	S	≤0.01
Mn	1.2-1.7				

Table 7. Design thickness under different working conditions for Q345R, unit: mm

D_i	200 ℃				250 ℃		300 ℃
mm	1.6 MPa	2.1 MPa	2.6 MPa	4.0 MPa	4.5 MPa	5.0 MPa	8.6 MPa
1000	5.49	7.22	8.96	15.20	18.08	20.10	40.76
1500	8.24	10.84	13.44	24.08	27.11	30.16	66.22
2000	10.99	14.45	19.21	32.10	38.63	42.97	88.29
2500	13.74	19.38	24.01	42.88	48.29	53.72	113.18
3000	17.70	23.25	28.81	51.46	57.95	69.22	135.82
3500	20.65	27.13	33.62	64.46	72.60	80.76	162.61
4000	23.60	31.00	40.83	73.66	82.97	92.29	185.84
4500	26.55	34.88	45.94	82.87	93.34	106.99	209.07
5000	29.50	41.18	51.04	92.08	106.86	118.88	232.30
5500	32.45	45.30	56.14	104.36	117.55	130.77	255.53
6000	35.40	49.42	65.35	113.85	128.24	142.65	278.76
6500	40.75	53.54	70.80	123.34	138.92	158.15	302.00
7000	43.89	57.66	76.25	132.83	149.61	170.32	325.23

Table 8. Maximum thermal power efficiency at different temperature drops from the hot to the cold tank

Temperature difference during discharge (^{o}C)	50	60	70	80	90	100
Oil inlet temperature (^{o}C)	227.23	224.40	221.18	218.37	215.59	212.86
Oil outlet temperature (^{o}C)	277.23	284.40	291.18	298.37	305.59	312.86
T_H (^{o}C)	227	226	225	224	223	222
Maximum thermal power efficiency (%)	13.23	13.13	13.02	12.91	12.80	12.68

Nomenclature

A	aperture area, m^2	**Subscripts**		
	surface area, mm^2	I	Cycle I	
a	half long axis, mm	II	Cycle II	
b	half short axis, mm	0	reference state	
C	total cost, RMB	1–8	state points	
D	diameter, mm	a	ambient	
G	solar radiation, W/m^2	b	binary phase/ beam/ built-in	
g	gravity, m/s^2	C	cold side	
H	height, mm	ch	characteristic	
h	enthalpy, kJ/kg	cy	cylinder	
	edge height of head, mm	F	friction	
M	mass, kg	g	generator/ static	
m	mass flow rate, kg/s	H	hot side/ hour	
P	cost per kilogram, RMB/kg	$head$	elliptical head	
p	pressure, MPa	i	diagram	
r	ratio	in	inlet	
T	temperature, ^oC	L	leakage	
V	total volume, mm^3	l	liquid phase	
v	specific volume, cm^3/kg	M	mechanical	
W	power output, kW	m	maximum	
δ	thickness, mm	net	net	

ε	device efficiency	oil	oil
ϕ	welding coefficient	op	optimum
γ	isentropic index	os	overall isentropic
η	system efficiency	out	outlet
$[\sigma]^t$	permissible stress, MPa	P	peak
ρ	density, kg/m^3	p	pressure/ pump
Abbreviation		pp	pinch-point
DSG	direct steam generation	S	shaft
HTF	heat transfer fluid	s	storage/isentropic/steam
HX	heat exchanger	$steel$	steel
ORC	organic Rankine cycle	su	supply
P	pump	T	thermal/ turbine
PCM	phase-change material	t	total mass flowrate
PTC	parabolic trough collector	TD	diagram
SE	screw expander	Th	theoretical
SEGS	solar electricity generation system	TI	isentropic
SORC	steam-organic Rankine cycle	TM	thermodynamic
SRC	steam Rankine cycle	v	volume
V	valve	w	water